Volume 1 | Number 1 | Jan 2013 | Pages 1–100

ChemComm

Chemical Communications
www.rsc.org/chemcomm

ROYAL SOCIETY OF CHEMISTRY

ROYAL SOCIETY OF CHEMISTRY

www.rsc.org/chemcomm

ChemComm

COMMUNICATION

Short-Wavelength Infrared Emitting Mutimodal Probe for Non-Invasive Visualization of Phagocyte Cell Migration in Living Mice

Y. Tsukasaki,[a] A. Komatsuzaki,[a] Y. Mori,[b,c] Q. Ma,[d] Y. Yoshioka [b,c] and T. Jin [a,b,e] *

For the non-invasive visualization of cell migration in deep tissues, we synthesized a short-wavelength infrared (SWIR) emitting multimodal probe that contains PbS/CdS quantum dots, rhodamine 6G and iron oxide nanoparticles. This probe enables multimodal (SWIR fluorescence/magnetic resonance) imaging of phagocyte cell migration in living mice.

Fluorescence imaging is an important modality for the non-invasive visualization of dynamic processes (*e.g.* cellular dynamics in immune reactions and cancer metastasis) in biological systems.[1] Of particular interest is the SWIR fluorescence imaging in the wavelength region of 1000 to 1500 nm,[2] which is expected to offer better spatio-temporal deep tissue images due to the lower auto-fluorescence and tissue scattering of SWIR light instead of the conventional near-infrared (NIR, 400-900 nm) light. Modeling studies have suggested that SWIR fluorescence imaging (at 1320 nm) would improve the signal to noise ratios by a factor of over 10 compared with NIR (at 850 nm) imaging.[3] For the SWIR fluorescence imaging of cellular dynamics in deep tissues, highly fluorescent probes that emit at 1000 to 1500 nm are needed.

So far, single-walled carbon nanotubes (SWNTs),[4] Ag_2S quantum dots (QDs),[5] and rare-earth-doped nanocomposites[6] have been used as SWIR fluorescent probes (quantum yield, QY: a few %)[4d] for deep tissue imaging. SWNTs have broad emission spectra in the wavelength from 1000 to 1600 nm with rod-like shapes with long molecular lengths (several hundreds of nanometers).[4] Compared with SWNTs, Ag_2S QDs are relatively small (<10 nm in diameter) and bright SWIR-emtting fluorescent probes with QY of 5.8 %.[5d] Rare-earth doped nanocomposites also act as SWIR-emitting probes (1185, 1310, 1475, and 1525 nm emission) by incorporation of the different rare-earth metal ions to $NaYF_4$ nanoparticles.[6] The QYs of rare-earth-doped (Er, Yb) solid-state materials are reported to be less than 2 %.[7] As an alternative SWIR-emitting material, we have chosen PbS/CdS QDs.[8] These QDs are highly fluorescent (QY, ~ 40%),[8d] and their emission wavelengths (1000-1500 nm) are easily controlled by changing the size of QDs.[8] Here, we report a SWIR-emtting multimodal probe[9] containing PbS/CdS QDs, rhodamine 6G (Rh6G) and Fe_3O_4 nanoparticles, that can be used for the non-invasive visualization of phagocyte cell migration[10] in living mice.

To develop the SWIR emitting multimodal probe for non-invasive imaging, we first examined the optical properties of a mouse at the whole body level. We conducted a qualitative analysis of fluorescence imaging of a mouse lymph system[11] using visible, NIR and SWIR emitting QDs (CdSe/ZnS,[12] CdSeTe/CdS,[13] and PbS/CdS,[14] Fig. S1-S3 in ESI) which are labeled with bovine serum albumin (BSA)[15] for reducing non-specific binding of the QDs to tissues (Fig 1). A mixture of each QD solution with normalized fluorescence intensities was directly injected into the mouse footpad and fluorescence images of the lymph system were taken (Fig. 1a). Autofluorescence of the mouse body dramatically decreases in the lymphangiography done by SWIR fluorescence imaging compared with that by conventional visible and NIR imaging (Fig. 1a and Fig. S4 in ESI). Lymph node images by SWIR fluorescence imaging, especially at 1100 and 1300 nm, are much clearer than those by visible and NIR imaging due to the higher penetration of the SWIR light in tissue. The weak fluorescence signal in the lymph node observed at 1500 nm results from the strong absorption of NIR light by water molecules (the right image in Fig. 1a and Fig. S5 in ESI). Even then, this signal is stronger than that of the imaging at 520 and 720 nm. It should be noted that the spatial-resolution of the lymph vessel in SWIR fluorescent imaging is improved by increasing the

[a] *RIKEN Quantitative Biology Center, 6-2-3 Furuedai, Suita, Osaka 565-0874, Japan. E-mail: tjin@riken.jp*
[b] *Immunology Frontier Research Center, Osaka University, Yamada-oka 1-3, Suita, Osaka 565-0871, Japan.*
[c] *Center for Information and Neural Networks, National Institute of Information and Communications Technology, and Osaka University, Yamada-oka 1-4, Suita, Osaka 565-0871, Japan.*
[d] *Department of Chemistry, Jilin University, Changchun 130012, China.*
[e] *Graduate School of Frontier Biosciences, Osaka University, Yamada-oka 2-1, Suita, Osaka 565-0871, Japan.*
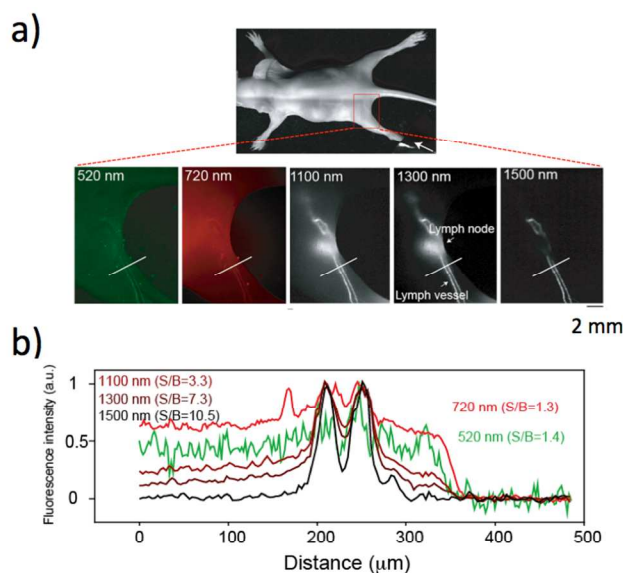
Fig. 1 (a) An image of a whole mouse body and fluorescence images of lymph vessels and a lymph node of the mouse. BSA-coated QDs (CdSe/ZnS; 520 nm emission, CdSeTe/CdS; 720 nm emission, and PbS/CdS; 1100, 1300, and 1500 nm emission) were injected into the footpad shown in the whole body image. The white lines in the fluorescence images are used for the line profile analysis in (b). Line profile analysis of the fluorescence intensities of the QDs in the lymph system. The values of S/B express signal to background ratios in the fluorescence intensities.

Fig. 2 (a) Schematic representation of the synthesis of SWIR-emitting multimodal probe containing PbS/CdS QDs, Rh 6G and Fe_3O_4 nanoparticles. (d) Size distribution of the particles in each step, determined in ethanol by dynamic light scattering. (c) Fluorescence spectra of the multimodal probe. The red and green line show the fluorescence emission resulting from PbS/CdS QDs and Rh6G, respectively (d) T_2^*-weighted MR images and T_2 relaxation rates (R_2, s^{-1}) as a function of the concentration (C) of the multimodal probe in water.

imaging wavelength, and the signal to background (S/B) ratio can be made 8 times better than that of the NIR imaging at 720 nm (Fig. 1b). The results show that SWIR fluorescence imaging of the mouse lymph system at 785 nm excitation/1300 nm emission gives a brightest image with a high S/B ratio to visualize both lymph vessels and a lymph node.

Based on the above finding on the optical property of a mouse lymph system, we have chosen PbS/CdS QDs with a 1300 nm emission for constructing SWIR emitting multimodal probe. PbS/CdS QDs were prepared by using a modified method based on previously reported procedures[8] (Experimental section in ESI). The synthetic procedure for the SWIR-emtting multimodal probe is shown in Fig. 2a. First, Fe_3O_4-doped silica particles were formed by using Fe_3O_4 nanoparticles and teraethylorthosilicate (TEOS).[16] Successively, PbS/CdS QDs and Rh6G were incorporated into the Fe_3O_4-doped silica particles *via* a silica shell formed by the hydrolysis of TEOS. Hydrodynamic diameter of the material in each step is shown in Fig. 2b. The resulting multimodal probe emits dual fluorescence at 1300 nm[17] and 520 nm resulting from PbS/CdS QDs and Rh6G as shown in Fig.2b. SWIR fluorescence of PbS/CdS QDs is used for the non-invasive visualization of phagocyte cell migration through lymph vessels, while visible fluorescence of Rh6G is used
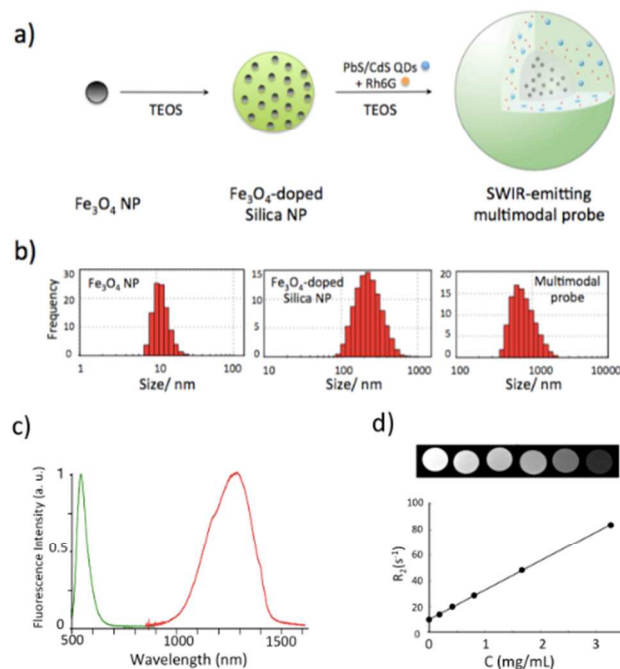
for the optical detection of phagocyte cells in tissue slice of a lymph node. The multimodal probe can also be used as a T_2 contrast agent for magnetic resonance imaging (MRI) of phagocyte cells in a lymph node. MRI contrast ability of the multimodal probe containing Fe_3O_4 was confirmed by T_1 and T_2 relaxometry measurements. For T_2-weighted (T_2-W) scans, the signal intensity is significantly reduced for higher concentrations of Fe_3O_4 (Fig. 2c). The $R_1(=1/T_1)$ and $R_2(=1/T_2)$ relaxivity values of the multimodal probe are 23 s^{-1} mg mL^{-1} and 0.0084 s^{-1} mg mL^{-1} (Fig. S6 in ESI), showing that the probe acts as a T_2 contrast agent for MRI. The hydrodynamic size of the multimodal probe in aqueous solution (10mg /mL BSA in PBS, pH = 7.4) was determined to be ca. 1 μm by dynamic light scattering (Fig. S7 in ESI). Paul et al. have reported that the engulfment times of spherical targets by phagocyte cells strongly depend on their size, and the silica beads with a 1.85 μm diameter are engulfed within 4 min.[18] Thus we expected that the SWIR-emitting multimodal probe can be effectively eaten by phagocyte cells. The SWIR-emitting multimodal probe shows low cytotoxicity in Hela cell under the concentration of less than 20 μg/mL (Fig. S8 in ESI).
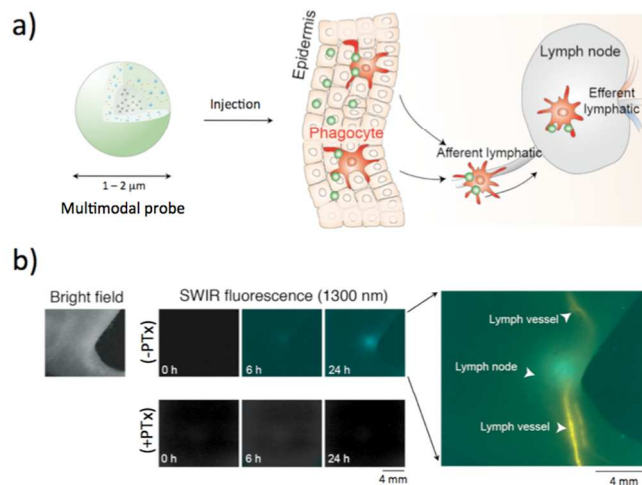
Fig. 3 (a) Schematic reprentation of phagocyte cell migration from a peripheral tissue to a lymph node. A multiodal probe was injected into the peripheral tissue, absorbed by phagocyte cells and transferred to the afferent lymphatic and lymph node. (b) Bright field image of the mouse foot observed (right). Timelapse images of SWIR fluorescence after injection of a multimodal probe containing PbS/CdS QDs with a 1300 nm emission into the mouse footpad in the presence and absence of cell migration inhibitor, PT_X (middel). A magnified image (right) of the lymph node and vessels with BSA-conjugated PbS/CdS QDs (yellow, 1100 nm emission) and multimodal probes containing PbS/CdS QDs (cyan, 1300 nm emission).

Phagocyte cells such as dendritic cells and macrophages are the body's gate keepers for guarding against foreign substances such as antigens and pathogens.[19] Non-invasive imaging of phagocyte cell migration *in vivo* can lead to a better understanding of pathophysiological situations including foreign substance induced contact dermatitis, allergy and viral infection. To date, non-invasive imaging modalities such as MRI, PET, and bioluminescence have been employed for visualizing phagocytosis dynamics *in vivo*.[10a] However, these modalities cannot be applied for the study of cellular dynamics with a high temporal resolution (< sec) in deep tissues. To overcome this drawback, we have developed multimodal (SWIR fluorescence and magnetic resonance) imaging techniques for visualizing phagocyte cell dynamics in a mouse lymph system. Fig. 3a shows schematic presentation of the migration of phagocyte cells containing multimodal probes through lymph vessels to a lymph node. Particle size is known to influence phagocytosis and permeability of the lymphatic wall.[20] Micrometer-sized particles cannot pass through the lymphatic wall, therefore requiring active transport by phagocyte cells.[21] For SWIR fluorescence imaging of the active transport, we used two types of probes: SWIR emitting multimodal probe (1.5 μm), and BSA-coated PbS/CdS QDs (10-20 nm). Both probes were injected into a mouse lymphatic system *via* the footpad of a mouse. BSA-coated QDs were quickly and passively transported from the footpad to a nearest lymph node with high permeability within 30 s (movie S1 in ESI). In contrast, the multimodal probe eaten by the phagocyte cells required up to 24 hours to complete the active transport, which is confirmed by an inhibitor of cell migration, PTx[22] (Fig. 3b). Alternatively we confirmed the migration of the phagocyte cells to a lymph node by MRI. As shown in Fig. 4a, the multimodal probes are detected inside the swelling lymph node at a depth of 1-2 mm. In addition, the localization of the probe in phagocyte cells is detected by immunohistochemical staining with visible fluorescence imaging of
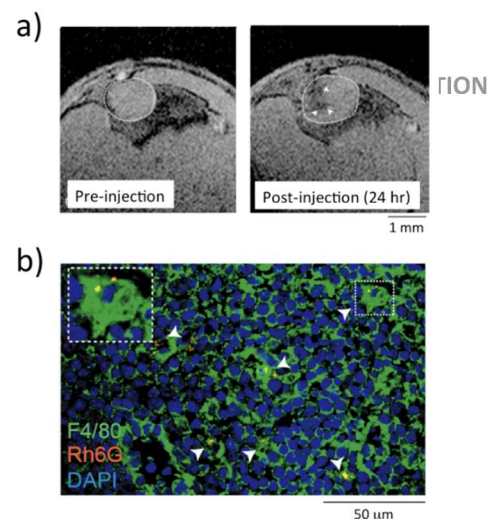

Fig. 4 (a) Magnetic resonance image of a lymph node before and 24 hours after injection of the multimodal probe containing iron oxide nanoparticles. A lymph node is shown by the white dotted circles. The white arrowheads show the phagocyte cells transferred into the lymph node. (b) Immunostainning image of the lymph node slice. The white arrowheads indicate phagocyte cells labeled with F4/80 antibodies, which contain the multimodal probe including Rh6G. Nuclei of the phagocyte cells are stained with DAPI. The inset is a magnification of the region inside the dotted white box.

a lymph node slice (Fig. 4b). The yellow dots in Fig. 4b shows F4/80 antibody (a cell marker) labeled phagocyte cells which contain multimodal probes emitting Rh6G fluorescence. These data show that the SWIR-emitting multimodal probe makes it possible to visualize the dynamics and localization of phagocyte cells in a mouse lymph system.
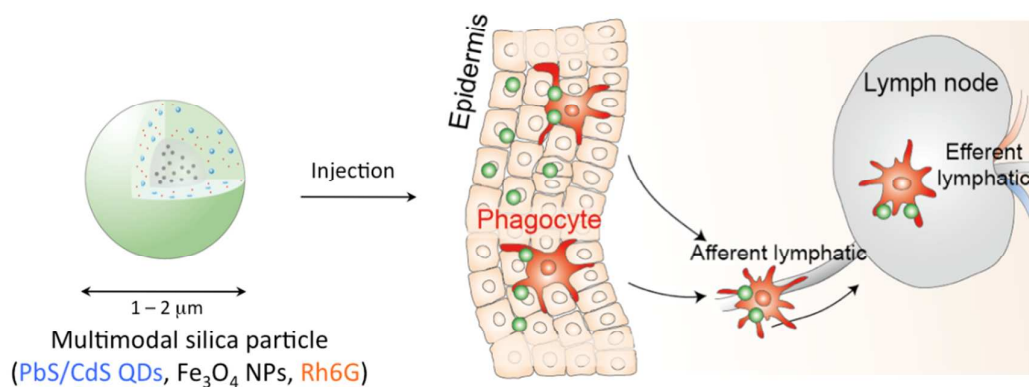
In conclusion, we demonstrate that the SWIR emitting multimodal probe can be applied to non-invasive imaging of phagocyte cell migration in a mouse lymph system. Furthermore, we demonstrate that magnetic resonance imaging using the SWIR emitting multimodal probe provides the location of phagocyte cells in the lymph system. Although many types of the multimodal probes combined with conventional NIR (700-900 nm) fluorescence and magnetic resonance have been reported,[9c,13] there are no SWIR fluorescence-based multimodal probes for non-invasive deep tissue imaging. By using a bright SWIR emitting PbS/CdS QDs for the construction of multimodal probes, we could achieve non-invasive fluorescence imaging of cellular dynamics in a lymph system. The emission wavelength of the multimodal probe is tunable by changing the PbS/CdS QDs with different fluorescence emissions. Thus the multimodal probe would enable to perform multiplexed SWIR fluorescence imaging for the study of cellular interaction *in vivo*.

Notes and references

1   (a) R. A Weissleder, *Nat. Biotechnol.,* 2001, **19**, 316-317; (b) J. V. Frangioni, *Curr. Opin. Chem. Biol.,* 2003, **7**, 626-634; (c) X. Gao, Y. Cui, R. M. Levenson and L. W. K. Chung, *Nat. Biotechnol.,* 2004, **22**, 969-976; (d) S. Kim, Y. T. Lim, E. G. Soltesz, A. M. Drand, D. J. Lee, A. Nakayama, J. A. Parker, T. R. Mihaljevic, G. D. Laurence, M. Dor, L. H. Cohn, M. G. Bawendi and J. V. Frangioni, *Nat. Biotechnol.,* 2004, **22**, 93-97; (e) X. Gao, L. Yang, J. A. Petros, F. F. Marshall, J. W. Simons and S. Nie, *Curr. Opin. Biotechnol.,* 2005, **16**, 63-72; (f) C. L. Amiot, S. Xu, S. Liang, L. Pan and J. X. Zhao, *Sensors,* 2008, **8**, 3038-3105.

2   (a) A. M. Smith, M. C. Mancini and S. Nie, *Nat. Nanotechnol.,* 2009, **4**, 710-711; (b) L. A. Sordillo, Y. Pu, S. Pratavieira, Y. Budansky and R. R. Alfano, *J. Biomed. Opt.,* 2014, **19**, 056004.

3   Y. T. Lim, S. Kim, A. Nakayama, N. E. Scott, M. G. Bawendi and J. V. Frangioni, Selection of Quantum Dot Wavelengths for Biomedical Assays and Imaging, *Mol. Imaging,* 2003, **2**, 50-64.

4   (a) M. J. O'Connell, S. M. Bachilo, C. B. Huffman, V. C. Moore, M. S. Strano, E. H. Haroz, K. L. Rialon, P. J. Boul, W. H. Noon, C. Kittrell, J. P. Ma, R. H. Hauge, R. B. Weisman and R. E. Smalley, *Science*, 2002, **297**, 593–596; (b) P. Cherukuri, S. M. Bachilo, S. H. Litovsky and R. B. Weisman, *J. Am. Chem. Soc.,* 2004, **126**, 15638–15639; (c) J. Lefebvre, D. G. Austing. J. Bond and P. Finnie, *Nano Lett.*, 2006, **6**, 1603–1608; (d) J. Crochet, M. Clemens and T. Hertel, *J. Am. Chem. Soc.,* 2007, **129**, 8058–8059; (e) T. K. Leeuw, R. M. Relth, R. A. Simonette, M. E. Harden, P. Cherukuri, D. A. Tsybouiski, K. M. Beckingham and R. B. Weisman, *Nano Lett.,* 2007, **9**, 2650–2654; (f) Z. Liu Z, W. Cai, L. He, N. Nakayama, K. Chen, X. Sun, X. Chen and K. Dai, *Nat. Biotechnol.*, 2007, **2**, 47–52; (g) H. Jin, D. A. Heller and M. S. Strano, *Nano Lett.*, 2008, **8**, 1577–1585; (h) K. Welsher, Z. Liu, D. Daranciang and H. Dai, *Nano Lett.*, 2008, **8**, 586–590; (i) H. Jin, D. A. Heller, R. Sharma and M. S. Strano, *ACS Nano*, 2009, **3**, 149–158; (j) K. Welsher, Z. Liu, S. P. Sherlock, J. T. Robinson, Z. Chen, D. Daranciang and H. Dai, *Nat. Nanotechnol.,* 2009, **4**, 773–780; (k) K. Weisher, S. P. Sherlocka, and H. Dai, *Proc. Natl. Acad. Sci. U. S. A.*, 2011, **108**, 8943-8948; (l) G. Hong, J. C. Lee, J. T. Robinson, U. Raaz, L. Xie, N. F. Huang, J. P. Cooke and H. Dai, *Nat. Med.,* 2012, **18**, 1841–1846; (m) H. Yi, D. Ghosh, M. H. Ham, J. Qi, P. W. Barone, M. S. Strano and A. M. Belcher, *Nano Lett*., 2012, **12**, 1176–1183; (n) J. T. Robinson, G. Hong, Y. Liang, B. Zhang, O. K. Yaghi, and H. Dai H, *J. Am. Chem. Soc.*, 2012, **134**, 10664–10669.

5   (a) Y. Du, B. Xu, T. Fu, M. Cai, F. Li, Y. Zhang and Q. Wang, *J. Am. Chem. Soc*., 2010, **132**, 1470-1471; (b) G. Hong, J. T. Robinson, Y. Zhang, S. Diao, A. L. Antaris, Q. Wang, H. Dai, *Angew. Chem. Int. Ed.*, 2012, **51**, 9818-9821; (c) P. Jiang, Z. Q. Tian, C. N. Zhu, Z. L. Zhang and D. W. Pang, *Chem. Mater.*, 2012, **24**, 3-5; (d) Y. Zhang, G. Hong, Y. Zhang, G. Chen, F. Li, H. Dai, and Q. Wang, *ACS Nano,* 2012, **5**, 3695-3702; (e) P. Jiang, C. N. Zhu, Z. L. Zhang, Z. Q. Tian and D. W. Pang, *Biomaterials*, 2012, **33**, 5130-5135; (f) H. Y. Yang, Y. W. Zhao, Z. Y. Zhang, H. M. Xiong and S. N. Yu, *Nanotechnology*, 2013, **24**, 055706; (g) Y. Zhang, Y. Zhang, G. Hong, W. Hei, K. Zhou, K. Yang, F. Li, G. Chen, Z. Liu, H. Dai, and Q. Wang, *Biomaterials*, 2013, **34**, 3639-3646; (h) Y. Zhang, Y. Liu, C. Li, X. Chen and Q. Wang, *J. Phys. Chem. C*, 2014, **118**, 4918-4923; (i) R. Gui, A. Wan, X. Liu, W. Yuan and H. Jin, *Nanoscale,* 2014, **6**, 5467-5473; (j) C. Li, Y. Zhang, M. Wang, Y. Zhang, G. Chen, L. Li, D. Wun and Q. Wang, *Biomaterials*, 2014, **35**, 393-400; (k) G. Chen, F. Tian, Y. Zhang, Y. Zhang, C. Li and Q.Wang, *Adv. Func. Mater.,* 2014, **24**, 2481-2488.

6   D. J. Naczynski, M. C. Tan, M. Zevon, B. Wall, J. Kohl, A. Kulesa, S. Chen, C. M. Roth, R. E. Riman and P. V. Moghe, *Nat. Commun.*, 2013, 4, 2199. DOI:10.1038/ ncomms3199.

7   (a) J. C. G. Bünzli, *Chem. Rev.,* 2010, **110**, 2729-2755; (b) (a) S. V. Eliseevaa and J.C. G. Bünzli, *Chem. Soc. Rev.,* 2010, **39**, 189-227.

8   (a) J. M. Pietryga, D. J. Werder, D. J. Williams, J. L. Casson, R. D. Schaller, V. I. Kilimov and J. A. Hollingsworth, *J. Am. Chem. Soc.,* 2008, **130**, 4879-4885; (b) H. Zhao, D. Wang, T. Zhang, M. Chaker and D. Ma, *Chem. Commun.*, 2010, **46**, 5301-5303; (c) M. S. Neo, N. G. Venkatram, S. Li, W. S. Chin and W. Ji, *J. Phys. Chem. C*, 2010, **114**, 18037-18044; (d) H. Zhao, M. Chaker, N. Wu and D. J. Ma, *J. Mater. Chem.,* 2011, **21**, 8898-8904; (e) H. Zhao, M. Chaker and D. Ma, *J. Mater. Chem*., 2011, **21**, 17483-17491; (f) M. V. Kovalenko, R. D. Schaller, D. Jarzab, M. A. Loi and D. V. Talapin, *J. Am. Chem. Soc.*, 2012, **134**, 2457-2460; (g) Y. Justo, P. K. Geiregat, V. Hoecke, F. Vanhaecke, C. D. M. Donega and Z. Hens, *J. Phys. Chem. C*, 2013, **117**, 20171-20177; (h) F. Ren, H. Zhao, F. Vetrone and D. Ma, *Nanoscale*, 2013, **5**, 7800-7804.

9   (a) R. Bakalova, Z. Zhelev, I. Aoki and I. Kanno, *Nat. Photonics*, 2007, **1**, 487-489; (b) J. Cheon and J. H. Lee, *Acc. Chem. Res.*, 2008, **41**, 1630-1640; (c) A. Louie, *Chem. Rev.*, 2010, **110**, 3146-3195.

10 (a) D. Baumjohann and M. B. Lutz, *Immnobiology*, 2006, **211**, 587-597; (b) W. Pham, J. Xie and J. C. Gore, *Neoplasia*, 2007, **9**, 1130-1137; (c) D. Sen, T. J. Deerinck, M. H. Ellisman, I. Parker and M. D. Cahalan, *PLoS On*e, 2008, **3**, e3290; (d) Y. W. Noh, Y. T. Lim and B. H. Chung, *FASEB J.,* 2008, **22**, 3908-3918; (e) Y. W. Noh, Y. S. Jang, K. J. Ahn, Y. T. Lim and B. H. Chung, *Biomateials*, 2011, **32**, 6254-6263.

11 H. Kobayashi, Y. Hama, Y. Koyama, T. Barrett, C. A. Regino, Y. Urano, P. L. Choyke, *Nano Lett*., 2007, **7**, 1711-1716.

12 Y. Nakane, A. Sasaki, M. Kinjo and T. Jin, *Analytical Methods*, 2012, **4**, 1903-1905.

13 Q. Ma, Y. Nakane, Y. Mori, M. Hasegawa, Y. Yoshioka, T. M. Watanabe, K. Gonda, N. Ohuchi and T. Jin, *Biomaterials*, 2012, **33**, 8486-8494.

14 Y. Tsukasaki, M. Morimatsu, G. Nishimura, T. Sakata, H. Yasuda, A. Komatsuzaki, T. M. Watanabe, and T. Jin, *RSC. Adv.,* 2014, 4, 41164, 41171.

15 M. Hasegawa, Y. Tsukasaki, T. Ohyanagi and T Jin, *Chem. Commun.*, 2013, **49**, 228-230.

16 Q. Ma, I. C. Serrano and E. Palomares, *Chem. Commun.*, 2011, **47**, 7071-7073.

17 The quantum yield of PbS/CdS QDs with an emission peak of 1300 nm was 0.42 in chloroform. See, ref 14.

18 D. Paul, S. Achouri, Y. Z. Yoon, J. Herre, C. E. Bryant and P. Cicuta, *Biophys. J.*, 2013, **105**, 1143-1150.

19 C. A. Jr. Janeway and R. Medzhitov, *Annu. Rev. Immunol.*, 2002, **20**, 197-216.

20 F. Ikomi, G. K. Hanna and G. W. Schmid-Schonbein, *Radiology*, 1995, **196**, 107-113.

21 (a) Y. L. Wu, Q. Ye, L. M. Foley, T. K. Hitchens, K. Sato, J. B. Williams, and C. Ho, *Proc. Natl. Acad. Sci. U.S.A.,* 2006, **103**, 1852-1857; (b) Y. Mori, M. Umeda, M. Fukunaga, K. Ogasawara and Y. Yoshioka, *Magn. Reson. Med. Sci.,* 2011, **10**, 219-227.

22 H. K. Lee, M. Zamora, M. M. Linehan, N. Iijima, D. Gonzalez, A. Haberman and A. Iwasaki, *J. Exp. Med.,* 2009, **206**, 359-370.

ChemComm Accepted Manuscript

Graphical abstract

Multimodal silica particle
($1-2\ \mu m$)
(PbS/CdS QDs, Fe_3O_4 NPs, Rh6G)

For the non-invasive visualization of phagocyte cell migration in a mouse lymph system, we developed a short-wavelength infrared (SWIR) emitting multimodal probe that contains PbS/CdS quantum dots, rhodamine 6G and iron oxide nanoparticles.